Biosensors and Bioelectronics 171 (2021) 112706

Contents lists available at ScienceDirect

Biosensors and Bioelectronics

journal homepage: http://www.elsevier.com/locate/bios

# Fuel strand-powered self-propelled electrochemical DNA machine for enzyme-free and distinctly amplified detection of nucleic acid with tunable performance

Zhen Zhao [1], Zhiqiang Chen [1], Dengren Liu, Li Wang, Shufeng Liu [*]

*Key Laboratory of Optic-Electric Sensing and Analytical Chemistry for Life Science, Ministry of Education, College of Chemistry and Molecular Engineering, Qingdao University of Science and Technology, 53 Zhengzhou Road, Qingdao, Shandong, 266042, China*

ARTICLE INFO

*Keywords:*
Self-propelled DNA machine
Strand displacement circuit
Signal amplification
Electrochemical detection
Biosensor

ABSTRACT

In this work, a self-propelled DNA machine was proposed for enzyme-free and ultrasensitive electrochemical detection of nucleic acid, which was based on a new strategy of the fuel strand-powered target recycling and successive proximity-based inter-strand displacement for distinct signal amplification. A three-strand duplex DNA (TSD) probe was immobilized onto electrode for target DNA recognition via a fuel strand-powered strand displacement circuit, accompanied with the target recycling and the association of fuel strand onto electrode for signal amplification and readout. The associated fuel strand contained a protruding tail sequence that could be used as a target analogy to activate the neighboring TSD probe based on the proximity-based inter-strand displacement effect, inducing the self-propelled association of fuel strand onto electrode for further signal amplification. The detection performance (dynamic response range, linear interval and detection limit) of current electrochemical DNA machine could be interestingly tuned by changing the tail sequence length of fuel strand, showing the potential for different analysis requirements. The lowest detection limit of 0.1 fM could be achieved, which was lower about two orders of magnitude than that by the typical fuel strand-powered target recycling strategy. Therefore, the developed sensing system exhibits a new, simple and powerful means for amplified detection of nucleic acid and may hold great potentials in bioanalysis, disease diagnosis and biomedicine.

## 1. Introduction

Development of nucleic acid detection methods suitable for the sensitive and accurate analysis of nucleic acid sequences with low abundance has been highly pursued to satisfy the ever-increasing demands in pathogen analysis, disease diagnosis and biomedicine (Craw and Balachandran, 2012; Das et al., 2015; Liu et al., 2020; Gerasimova and Kolpashchikov, 2014; Lin et al., 2016). Polymerase chain reaction (PCR) is the most widely used method for nucleic acid analysis (Hindson et al., 2013; Bachman, 2013; Navarro et al., 2015). But the stringent temperature control and primer design is necessary and operated by the skilled technicians. It is also more easily challenged by false-positive or -negative error outputs, limiting its wide applications to some extent, especially in resource-constrained regions. Thus, the development of simple and cost-effective amplified strategy for sensitive and accurate detection of nucleic acid is highly desirable.

DNA machines had attracted great attention for the analysis of nucleic acid or nucleic acid-related analytes since they could autonomously and progressively operate in response to the external input without human intervention (von Delius and Leigh, 2011; Zhou et al., 2020; Bath and Turberfield, 2007; Yao et al., 2020). Various nucleases such as endonucleases, exonucleases, and polymerases were often used as the driving force for DNA machine operation (Yang et al., 2016; Liu et al., 2019; Qu et al., 2017; Chen et al., 2015; Shen et al., 2018). However, the protein enzyme was not stable and relatively expensive. Also, in the case for the sensitivity improvement, the relatively rigorous sequence design or multiple DNA probes were usually necessary, which would more easily induce non-specific background signal amplification to interfere with the accurate analysis of low abundance of targets. Compared with the nucleases, the DNA strand displacement was the

* Corresponding author.
*E-mail address:* sliu@qust.edu.cn (S. Liu).
[1] Both authors contribute this work equally.

https://doi.org/10.1016/j.bios.2020.112706
Received 7 August 2020; Received in revised form 17 September 2020; Accepted 6 October 2020
Available online 7 October 2020

promising alternative for construction of enzyme-free DNA circuits or machines (Jung and Ellington, 2014; Qian and Winfree, 2011; Sun et al., 2018). Toehold-mediated strand displacement was considered as a powerful means for the DNA hybridization, assembly or the design of DNA circuits (Srinivas et al., 2013; Simmel et al., 2019; Zhu et al., 2013; Khodakov et al., 2013). It showed the advantages such as easy to design, improved discrimination selectivity, and programmable and controllable strand displacement kinetics. The typical enzyme-free catalytic DNA circuits or machines by toehold-mediated strand displacement reaction included catalytic hairpin assembly, fuel strand-powered target recycling and hybridization chain reaction (Yin et al., 2008; Yun et al., 2016; Dirks and Pierce, 2004). In the strategies of catalytic DNA hairpin and hybridization chain reaction, the assembly components possessed too much complementary base sequences, which increased the design complexity for bioanalysis and easily incurred non-specific cross reactions. Since its firstly proposed, fuel strand-powered target recycling or entropy-driven target recycling strategy had attracted a great deal of attentions for the development of biosensors and catalytic DNA circuits (Yurke et al., 2000; Wang et al., 2018; Zhang et al., 2007; Yang et al., 2018; Kim et al., 2016). The salient advantage for it lied in that the sequence design was very easy and flexible to adapt different analysis requirement and thus also beneficial for the background response suppression. However, its detection performance especially sensitivity was usually limited owing to its relatively slow strand displacement process. Furthermore, the concatenated DNA circuits or the combination of multiple DNA circuits were also designed for sensitivity improvement. But they were often confronted with too complicated sequence design or assay procedure (Dai et al., 2017; Wang et al., 2018; Shang et al., 2020; Chu et al., 2019; Xiong et al., 2019). In this context, the development of simple, rapid, high sensitive and enzyme-free DNA machine or circuit was still in high demand for the profiling of low abundance of target analyte.

Herein, a new strategy of fuel strand-powered target recycling and successive proximity-based inter-strand displacement was proposed to fabricate an enzyme-free electrochemical DNA machine for the amplified detection of nucleic acid. It was developed on the basis of a typical fuel strand-powered target recycling strategy. The pivotal point was the design of fuel strand, which was configured with an extended tail sequence at 3′-terminus that was partially same with the target DNA sequence and considered as target analogy. A three-strand duplex DNA probe (TSD) was prepared and immobilized onto electrode as a bio-recognition element. In the absence of target DNA, the coexisting fuel strand and TSD probe could not interact mutually. Upon addition of target DNA, it firstly operated with the TSD probe according to a typical fuel strand-powered target recycling principle. More specifically, two cascade toehold-mediated strand displacement reactions occurred onto the TSD probe, resulting into the target recycling and the association of fuel strand onto electrode for signal amplification. Then, as for the associated fuel strand, its protruding tail sequence could activate the neighboring TSD probe based on the proximity-based inter-strand displacement effect, which might be attributed to the increased local concentration of the tail sequence at 3′-terminus of fuel strand for the enhanced hybridization stability with the adjacent TSD (Liu et al., 2017; Li et al., 2016). Thus, the successive self-propelled DNA machine proceeded with the on-going association of fuel strands onto electrode, accelerating the detection process and inducing the distinct signal amplification toward target recognition event. Current fuel strand-powered target recycling and inter-strand displacement strategy demonstrated several salient advantages: 1) The self-propelled walking operation for the associated fuel strand provided a distinct signal amplification capability; 2) It was cost-effective and more stable owing to its enzyme-free strand displacement principle; 3) The relatively simple and flexible sequence design may be benefit for background response suppression; 4) More importantly, the detection performance toward target DNA could be easily tuned by changing the tail sequence length of fuel strands, showing the potential for different analysis requirements.

## 2. Experimental section

### 2.1. Chemicals and materials

Tris(2-carboxyethyl) phosphine hydrochloride (TCEP), hexaammineruthenium (III) chloride ($[Ru(NH_3)_6]^{3+}$, RuHex) and 6-mercaptohexanol (MCH) were purchased from Sigm-Aldrich (St. Louis, MO, USA). Other reagents (analytical grade) were used as received. The HPLC-purified DNA sequences were synthesized by Sangon Biotech. Co., Ltd. (Shanghai, China) and shown in Table S1. All solutions were prepared using ultrapure water (resistivity of 18.2 MΩ·cm).

### 2.2. TSD probe preparation and immobilization

Three-strand duplex DNA (TSD) probe was firstly prepared based on the following process. The thiolated template sequence (TS, 1 μM), assistant DNA sequence (AS, 1.2 μM), and protective DNA sequence (PS, 1.2 μM) were mixed in 20 mM Tris-HCl buffer (pH 7.4, 100 mM NaCl, 1 mM EDTA), heated to 90 °C for 10 min and then allowed to cool down to room temperature for at least 60 min to form the three-strand DNA duplex (TSD) probe.

Prior to TSD probe immobilization, the gold electrodes (2 mm diameter) were pretreated according to the following procedures. The electrodes were firstly immersed into a fresh piranha solution (a mixture of concentrated $H_2SO_4$ and $H_2O_2$ at the volume ratio of 3:1) for 10 min to remove any possible organic pollutes. After thorough rinsing with ultrapure water, the electrodes were polished with 0.3 and 0.05 μm alumina oxide slurries each for 5 min, respectively, followed by rinsing with ultrapure water and sequential sonication in water, ethanol, and water for 5 min to remove residual alumina powder on the electrode surface. Next, the electrodes were electrochemically scanned in 0.5 M $H_2SO_4$ solution within a potential window between −0.2 and + 1.5 V at a scan rate of 100 mV/s until a stable cyclic voltammogram curve was obtained. Finally, the pretreated electrodes were rinsed with water and dried under nitrogen stream.

Then, TSD probes were treated with 10 mM TCEP for 1 h to reduce the disulfide bonds and diluted with 20 mM Tris-HCl (pH 7.4, 100 mM NaCl, 1 mM EDTA) to different concentrations. After that, the treated electrodes were immersed into 50 μL of the above TSD probe for 12 h at room temperature and subsequently rinsed with 20 mM Tris-HCl buffer. The resulting modified electrodes were blocked with 1 mM MCH solution for 30 min to remove the possible nonspecific adsorbed probes.

### 2.3. Amplified DNA detection

The detection of target DNA was operated by incubating the TSD probe modified electrodes into 50 μL of 10 mM Tris-HCl (pH 7.4, 0.1 M NaCl, 12.5 mM $MgCl_2$, 1 mM EDTA) buffer containing fuel strand (0.5 μM) and different concentrations of target DNA at 37 °C for 2 h. After that, the electrodes were washed with 20 mM Tris-HCl buffer and dried for electrochemical measurements.

### 2.4. Electrochemical measurements

All electrochemical experiments were performed with a CHI 660E electrochemical workstation (CH Instruments, Shanghai, China) at room temperature by using a three-electrode system consisting of the modified gold electrode, a platinum wire auxiliary electrode, and a Ag/AgCl reference electrode. Square wave voltammetry (SWV) was obtained in 10 mM Tris-HCl buffer (pH 7.4, 0.1 M NaCl) from −0.5 to 0 V with an amplitude of 25 mV, a step potential of 4 mV and a frequency of 25 Hz. Cyclic voltammetry (CV) scan from −0.6 to 0.1 V was performed at a scan rate of 100 mV/s. Electrochemical impedance spectra (EIS) was carried out in 10 mM PBS (pH 7.4, 1 M KCl) solution containing 5 mM $[Fe(CN)_6]^{3-/4-}$ with the frequency range from 0.1 Hz to 10 kHz. Cyclic voltammetry (CV) curves were also recorded with the potential window

from −0.1 to 0.6 V at a scan rate of 100 mV/s. The chronocoulometry scans were operated in a fresh 10 mM Tris-HCl (pH 7.4) containing 50 μM RuHex at room temperature with the corresponding parameters: initial potential of 0.5 V, final potential of 0 V, pulse width of 0.25 s and sample interval of $2.5 \times 10^{-4}$ s.

### 2.5. Polyacrylamide gel electrophoresis

A 17.5% polyacrylamide gel was prepared by mixing 3.5 mL of 40% gel solution (39:1), 160 μL 50 × TAE Buffer, 80 μL 10% APS, 4 μL TEMED and 4256 μL deionized water. Then, the polyacrylamide gel electrophoresis (PAGE) experiment was carried out in 1 × TAE buffer at 180 V for 3 min and 135 V for 90 min. Afterward, the gels were scanned using a FR-980A gel image analysis system(Shanghai, China).

## 3. Results and discussion

### 3.1. Biosensing principle of the self-propelled DNA machine

Current self-propelled DNA machine was designed based on a new fuel strand-powered target recycling and inter-strand displacement strategy (Scheme 1B). It was built on a typical fuel strand-powered target recycling strategy. For the typical fuel strand-powered target recycling strategy, the operation principle was illustrated in Scheme 1A. A three-strand duplex (TSD) probe was firstly obtained by annealing a thiolated template DNA strand (TS), an assistant DNA strand (AS), and a protective DNA strand (PS). Then, it was assembled onto electrode surface via the formation of an Au–S bond, followed by backfilling with MCH. The designed TSD probe contained two toehold regions: one toehold region (6-nt) was located at the distal 5′-terminus of the TS; another one was situated in the middle of the TS but was initially blocked by PS. The target DNA docked at the toehold region of TS and triggered the first toehold-mediated strand displacement reaction to release the PS. Then, the second toehold region (4-nt) was exposed and the methylene blue (MB)-labeled fuel strand could trigger the second toehold-mediated strand displacement reaction from this exposed toehold region, following the release of target DNA and AS. The released target DNA was recycled to convert the original TSD probe into the duplex DNA between the TS and fuel strand for signal amplification. In current proposed fuel strand-powered target recycling and inter-strand displacement strategy, the fuel strand was configured with an extended tail sequence at 3′-terminus that was partially same with the target sequences. Such an extended tail sequence at 3′-terminus of fuel strand could be considered as target analogy, which was spaced by the numerous thymine bases (poly-T) to provide the suitable freedom. In the absence of target DNA, such a tail sequence (target analogy) at 3′-terminus of fuel strand could not effectively activate the TSD probe owing to the too short toehold region between them. In the presence of target DNA, target DNA could convert the initial TSD probe into the duplex DNA between the TS and fuel strand. For the associated fuel strand onto electrode, its protruding tail sequence (target analogy) at 3′-terminus could swimmingly approach the adjacent TSD probe and displace the PS from the TSD probe via a proximity-based inter-strand displacement effect. Such a proximity-based inter-strand displacement might be attributed to the increased local concentration of the tail sequence for the enhanced hybridization stability with the adjacent TSD. Then, the new fuel strand could be successively annealed with TS via the cascade toehold-mediated strand displacement reaction, accompanied with the release of target analogy. The released target analogy and the new annealed fuel strand could further trigger the proximity-based inter-strand displacement for the distinct signal amplification toward the initial target recognition events. Thus, the fuel strand in this strategy showed two kinds of roles: Firstly, it operated as in the typical fuel strand-powered target recycling strategy for signal amplification and also signal readout (an electroactive label of methylene blue was labeled at 5′-terminus of fuel strand). Secondly, the associated fuel strand could work as a DNA walker. Its tail sequence could approach and activate the adjacent TSD probe, inducing the self-propelled association of fuel strand with TS for further signal amplification. Thus, the current strategy provided an enzyme-free and self-propelled DNA amplification means for sensitive detection of nucleic acid.

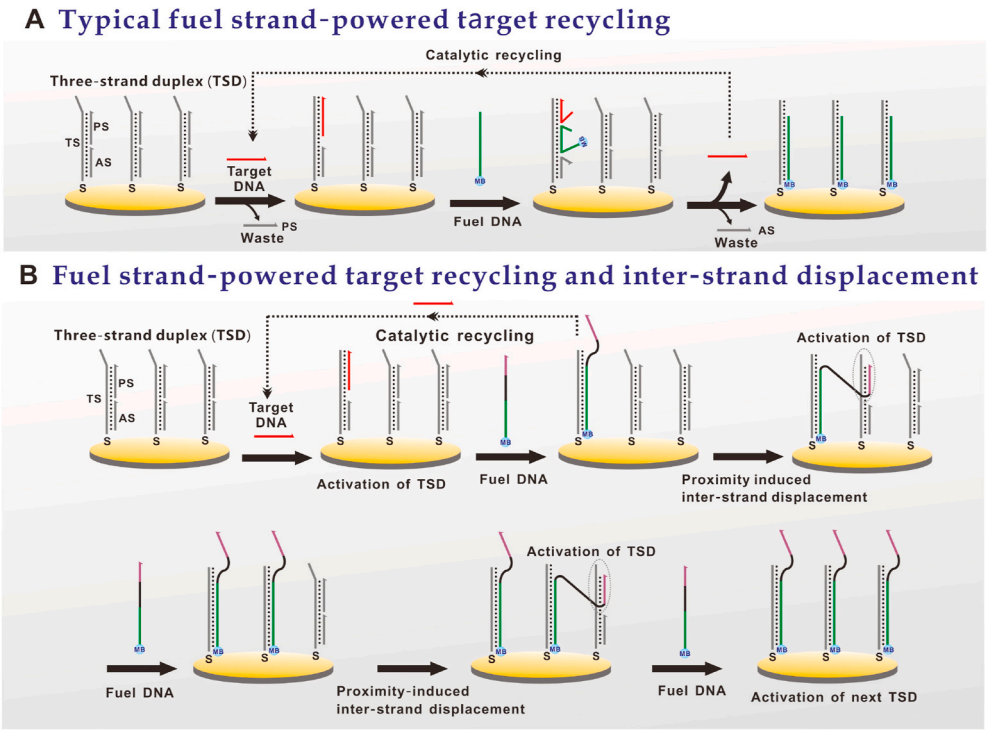


**Scheme 1.** Schematic illustration of a typical fuel strand-powered target recycling strategy (A), and current fuel strand-powered target recycling and proximity-based inter-strand displacement strategy for signal amplification (B).

### 3.2. Detection feasibility of nucleic acid

Considered with the role of fuel strand in current strategy, it should not directly recognize with the TSD probe in the absence of target DNA. But it could activate the adjacent TSD probe once it was associated onto electrode in the presence of target DNA. Thus, the extended tail sequences (target analogy) at 3′-terminus of fuel strand should be carefully designed. Since target DNA recognized with the TS in TSD probe via a 6-nt toehold region. Thus, the tail sequence at 3′-terminus of fuel strand should have a toehold region less than 6-nt in order to avoid its direct recognition with the TSD probe in the absence of target DNA. The fuel strands with different tail base sequences were designed (denoted as FS-2, FS-3, FS-4 and FS-5) to verify their proximity-based inter-strand displacement effect for signal amplification. The numbers in FS-2, FS-3, FS-4 and FS-5 represented the base numbers in the toehold region between the tail sequences (target analogy) of fuel strand and the TS in TSD probe. Also, the fuel strand with no extended tail sequences (denoted as FS) was employed for the typical fuel strand-powered target recycling strategy as a comparison. The corresponding square wave voltammetry (SWV) responses in the absence and presence of target DNA (0.2 pM) were shown in Fig. 1. The signal responses toward target DNA by using FS-3 (Fig. 1C), FS-4 (Fig. 1D) and FS-5 (Fig. 1E) as the fuel strand were evidently larger than that by using FS (Fig. 1A), suggesting that the extended tail sequence might promote the inter-strand displacement for further signal amplification after they were associated onto electrode. But the signal response by using FS-2 (Fig. 1B) was reduced compared with that by using FS. Thus, the associated FS-2 was difficult to further trigger the inter-strand displacement reaction because of its too short toehold (2 nt) with the TS. However, the increased steric hindrance from the extended tail sequences of the associated FS-2 might restrict the target recognition and the cascade toehold-mediated strand displacement reactions to some extent for the signal response decrease. Also, the background responses by using the fuel strands of FS-2, FS-3 and FS-4 were only slightly larger than that by using FS. The signal leaking might be attributed to the possible hybridization of fuel strands with a tiny amount of denatured or improperly-annealed TSD probes onto electrode. To support it, the MCH monolayer modified electrode was also prepared for a comparison with the TSD and MCH monolayer modified electrode (Fig. S1). Almost no electrochemical responses were measured for the MCH monolayer modified electrode after its incubation with fuel strand (FS-4), indicating the negligible non-specific adsorption of fuel strands onto electrode surface. A large background response in the case of FS-5 indicated that the FS-5 could directly hybridize with the TSD probe via a toehold-mediated strand displacement reaction. The signal and background responses at different fuel strands were obtained (Fig. 1F). The signal to background ratios toward 0.2 pM target DNA by using FS, FS-2, FS-3, FS-4 and FS-5 as fuel strands, respectively, were calculated as about 4.48, 2.09, 5.37, 5.81, and 1.78, respectively. Too short toehold for example FS-2 could not effectively improve the detection performance. Also, too long toehold for example FS-5 could induce a too large background response. Since the current response was originated from the methylene blue (MB) labeled at fuel strand, the absolute current intensities might be smaller than those enzymes, nanoparticles, or redox species (in the solution)-based signal readout system. But the developed strategy showed a good signal to background ratio for target discrimination (especially for FS-3 and FS-4), making it to be promising for the biosensor device fabrication and applications. In the following study, the FS-4 was mainly used to explore the detection performance toward target DNA owing to its best electrochemical response.

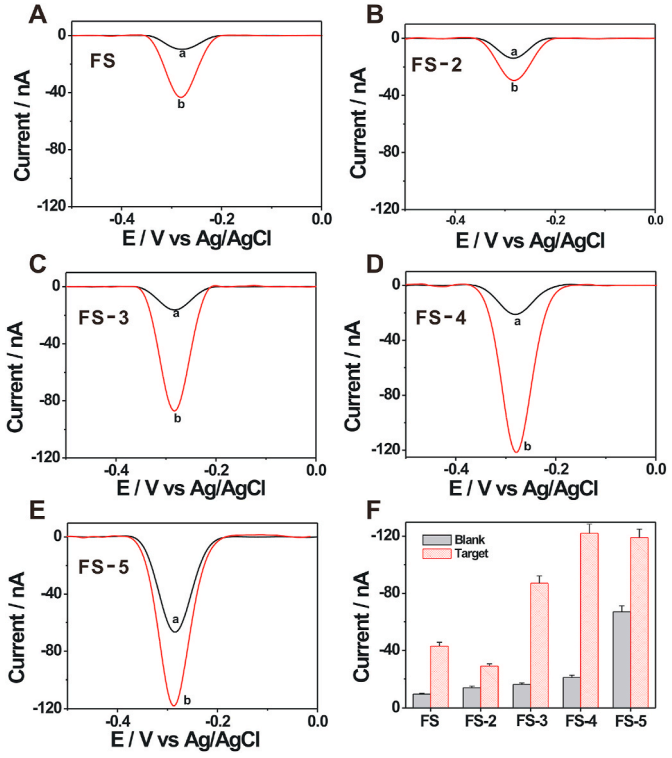


**Fig. 1.** SWV responses toward blank (a) and 0.2 pM target DNA (curve b) in 10 mM Tris-HCl buffer (pH 7.4, 0.1 M NaCl) by using different fuel DNA strands including FS (A), FS-2 (B), FS-3 (C), FS-4 (D) and FS-5 (E). (F) The bar chart for the corresponding electrochemical response values in the presence and absence of target DNA. The concentrations of fuel strands were all 0.5 μM.

The fuel strand-powered target recycling and inter-strand displacement process was also monitored by following the electrochemical signal response with time, and compared with the typical fuel strand-powered target recycling process (Fig. 2A). By using FS for a typical enzyme-free target recycling strategy, the electrochemical response increased gradually with reaction time according to a basic linear amplification mode (green line in Fig. 2A). However, when the FS-4 was used as a fuel strand, the electrochemical responses were obviously larger than that by using FS in the studied time range. Also, the increment of electrochemical response speeded up after about 60 min. This might be that, as the reaction proceeded, the continually associated FS-4 triggered the proximity-based inter-strand displacement to accelerate the reaction process. After about 120 min, the increment of electrochemical response slowed down evidently, suggesting the consumption of the TSD probe for the reduction of reaction rate. In the absence of target DNA, both the electrochemical responses of the system by using FS or FS-4 as fuel strands increased very slowly with time. But the background response in the case of FS-4 was larger than that in the case of FS. Also an evident increase of background response could be found after about 90 min. It could be understood that the FS-4 had a 4-nt toehold with the TSD probe, which might induce the recognition with the TSD probe to some extent for a relatively large background response. In the following study, 120 min was chosen as the optimized reaction time. It should be noted that a shorter time less than 120 min could also work well for target discrimination.

To further verify that the distinct electrochemical response in the case of FS-4 as a fuel strand was aroused by the proximity-based inter-strand displacement effect, we also used another target sequence (target-4) as a comparison (Fig. 2B). The target-4 possessed the same base sequences with the extended tail sequences (target analogy) at 3′-terminus of FS-4, and could form a four-base toehold with the TSD probe. It could be found that, in the case of target-4, only the small electrochemical responses could be obtained whether by using FS or FS-4 as the fuel strands, indicating that 4-nt toehold for target-4 or FS-4 with the TSD probe was relatively difficult to trigger the toehold-mediated strand displacement reaction. However, after the annealing of FS-4 onto the electrode in the presence of target DNA, the 4-nt toehold for FS-4 with the adjacent TSD probe could be effective to induce the proximity-based

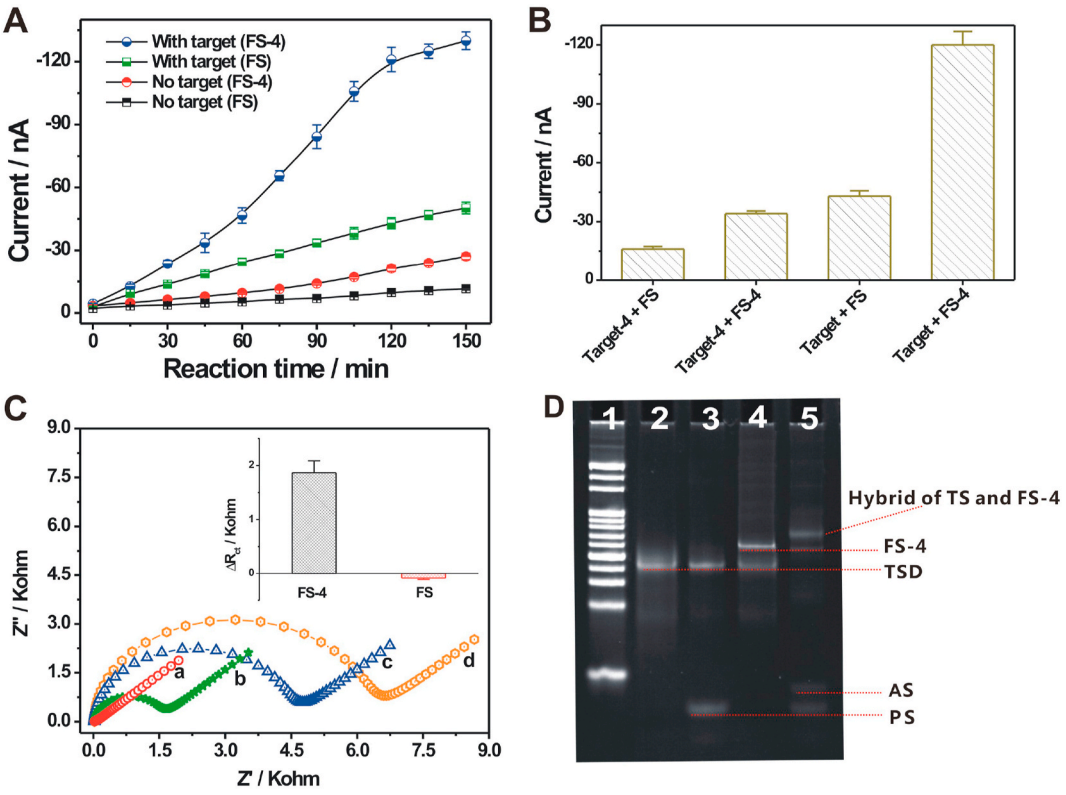


**Fig. 2.** (A) Time dependence of electrochemical responses in the absence and presence of 0.2 pM target DNA by using FS and FS-4 as the fuel strands, respectively. (B) Electrochemical response comparison toward target or target-4 in the presence of FS or FS-4. The target-4 shows a toehold region (4-nt) with the TSD probe. (C) Electrochemical impedance spectroscopy recorded in 10 mM PBS (pH 7.4, 1 M KCl) and 5 mM $[Fe(CN)_6]^{3-/4-}$ solution for the modified electrodes: bare gold electrode (a), TSD probe immobilized (b), further modification with MCH (c), and incubation with 0.2 pM target in the presence of 0.5 μM FS-4 (d). Inset shows the charge transfer resistance (Rct) change by using FS-4 or FS as the fuel strand in the presence and absence of target. (D) Non-denaturing PAGE analysis: DNA marker (lane 1), 0.5 μM TSD probe (lane 2), 0.5 μM TSD probe +0.5 μM target (lane 3), 0.5 μM TSD probe +0.5 μM FS-4 (lane 4), 0.5 μM TSD probe +0.5 μM target + 0.5 μM FS-4 (lane 5).

inter-strand displacement for the evidently enhanced electrochemical response than that by FS.

The biosensor fabrication process based on the fuel strand-powered target recycling and inter-strand displacement strategy was also followed by the electrochemical impedance spectroscopy (Fig. 2C) and cyclic voltammetry methods (Fig. S2) with the use of $[Fe(CN)_6]^{3-/4-}$ as a classical electrochemical probe. The bare gold electrode exhibited an almost straight line and the charge transfer resistance ($R_{ct}$) was about 40 Ω (curve a), indicating an excellent electrical conductivity of electrode. After the self-assembly of TSD probe on the electrode surface (curve b), the Rct value was increased to be about 1684 Ω, which could be attributed that the negative-charged DNA phosphate skeleton prevented the approaching of $[Fe(CN)_6]^{3-/4-}$ from the electrode surface. After further blocking with MCH monolayer, the formed densely packed monolayer further inhibits the diffusion of $[Fe(CN)_6]^{3-/4-}$ toward electrode surface, inducing an continually increased Rct value of about 4608 Ω (curve c). Upon addition of target DNA (0.2 pM) and FS-4, the Rct value was further increased to be about 6474 Ω (curve d). The Rct increase could be attributed to the introduced FS-4 that possessed an extended tail sequence to offer an additional electrostatic and steric repellence for the approaching of $[Fe(CN)_6]^{3-/4-}$ toward electrode surface. As a comparison, no evident Rct change was observed in the presence of FS and target DNA (inset in Fig. 2C). This was because that the associated FS in the presence of target DNA didn't induce the change of base sequences or length compared with the initial TSD probe. The cyclic voltammetry results were in well accordance with the electrochemical impedance spectroscopy experiments, supporting the biosensor fabrication process together.

The gel electrophoresis experiments were also used to verify the target-triggered annealing process of FS-4 with the TSD probe (Fig. 2D). The obtained TSD probe shows a clear migration band (lane 2). When the target DNA was introduced, the first toehold-mediated strand displacement reaction between target DNA and TSD probe occurred with the release of PS, which could be observed with a new band (lane 3). When the fuel strand (FS-4) was mixed with the TSD probe but no target DNA, the cascade toehold-mediated strand displacement reactions were inhibited, and only the bands for TSD probe and FS-4 were observed (lane 4). In the presence of target DNA and FS-4, almost all TSD probes were converted into the hybrid of FS-4 and TS, accompanied with the released AS and PS (lane 5). The gel electrophoresis experiments supported the target DNA initiated and FS-4 powered cascade toehold-mediated strand displacement reaction process.

### 3.3. Optimization of experimental conditions

The target-triggered cascade toehold-mediated strand displacement reactions and the proximity-based inter-strand displacement process may be influenced by the surface assembly of the TSD probe. Thus, the assembly density of the TSD probe was studied. It could be found from Fig. 3A that the electrochemical signal response ($\Delta I = I - I_0$; I and $I_0$ represented the electrochemical signal in the presence and absence of target DNA, respectively) increased with the immobilization concentration of TSD probe from 0.1 to 0.5 μM and reached almost a maximum value at 0.5 μM. The further increased immobilization concentration of TSD (over 1 μM) deteriorated the electrochemical response toward target DNA. A low immobilization amount of TSD probe would be not beneficial for the detection efficiency of the sensor toward target DNA. However, a high immobilization amount of TSD probe might exhibit the

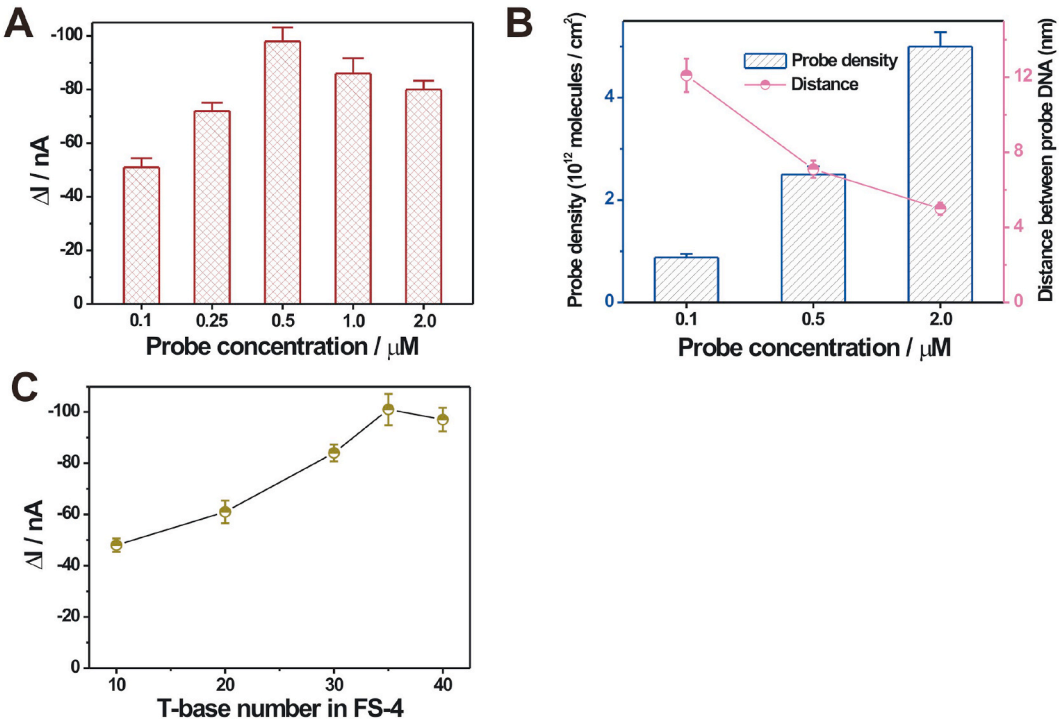


**Fig. 3.** (A) Optimization of immobilization concentration of TSD probe. The used probes concentrations were 0.1, 0.25, 0.5, 1.0 and 2.0 μM, respectively. (B) Surface assembly density of TSD probe and the average distance between TSD probes obtained at different TSD probe concentrations (0.1, 0.5 and 2 μM). (C) Optimization of the base number for the poly-T spacer in the FS-4. Different T base numbers (10, 20, 30, 35 and 40) were used. Target DNA concentration was 0.2 pM. The concentration of FS-4 was 0.5 μM. The error bars were obtained based on at least three repetitive experiments.

steric hindrance for target recognition, cascade toehold-mediated strand displacement and proximity-based inter-strand displacement process. Thus, an immobilization concentration of 0.5 μM TSD probe was most suitable for biosensor fabrication. Furthermore, the assembly density of TSD probe onto electrode could be obtained according to the reported chronocoulometry method via the use of RuHex as a redox probe (Steel et al., 1998). The typical chronocoulometric curves for the immobilized TSD probe and MCH electrodes in the absence and presence of RuHex (50 μM) were shown in Fig. S3. The assembly density for TSD probe at three immobilization concentrations (0.1, 0.5 and 2 μM) was then studied (Fig. 3B). The assembly densities for 0.1, 0.5 and 2 μM TSD probe were obtained as about $0.86 \times 10^{12}$, $2.5 \times 10^{12}$, and $5.0 \times 10^{12}$ molecules/cm$^2$, respectively. The relative standard deviation of the assembly density at an optimum immobilization concentration of 0.5 μM TSD probe was obtained as about 6.4% based on at least three repetitive experiments. Thus, the DNA biosensor fabrication process could be basically controllable. Furthermore, the average distance between the adjacent TSD probes was estimated as 12.16 nm, 7.13 nm and 5.04 nm, respectively, at 0.1, 0.5 and 2 μM TSD probe (Mahshid et al., 2015). To make sure that the tail sequences at 3′-terminus of FS-4 could move freely for recognition with the adjacent TSD probe, a number of thymine (T) bases were introduced as spacer. The base number for the poly-T spacer was optimized and the results were shown in Fig. 3C. The poly-T spacer with 35 nt showed a better electrochemical response than other base numbers. Considered with the average distance between TSD probes of 7.13 nm in the case of 0.5 μM immobilization concentration of TSD probe, the poly-T spacer of 35 nt (about length of 11.9 nm) would be effective for the proximity-based inter-strand displacement reaction between the associated FS-4 and the adjacent TSD probe.

### 3.4. *Detection performance of the developed electrochemical DNA biosensor*

The analytical performance toward target DNA by the fabricated fuel strand-powered target recycling and inter-strand displacement strategy was then investigated. Interestingly, the detection performance toward target DNA could be easily tuned with the use of different fuel strands. The electrochemical responses toward different concentrations of target DNA by using different fuel strands were shown in Fig. 4A–E. The corresponding calibration curves at different fuel strands were all shown in Fig. 4F. In the case of FS, the target detection was based on a typical fuel strand-powered target recycling strategy. The dynamic response range for target DNA was obtained from 10 fM to 50 pM (Fig. 4A). The linear range for target DNA was from 10 to 200 fM with a regression equation of I (SWV peak current, nA) = −14.33–0.145 C (target DNA concentration, fM) and a regression coefficient of 0.9951 (Fig. 5A). A low concentration of 10 fM could be detected by using FS as the fuel strand. In the case of FS-2, the dynamic response range for target DNA was obtained from 50 fM to 50 pM (Fig. 4B). The linear detection range was from 50 fM to 1 pM with a regression equation of I = −15.54–0.067 C and a regression coefficient of 0.9989 (Fig. 5B). The low detection concentration for target DNA by using FS-2 was only about 50 fM. The detection performance by using FS-2 was inferior to that by using FS, which might be attributed that the 2 nt toehold between the associated FS-2 and the adjacent TSD probe was too short to trigger the proximity-based inter-strand displacement reaction for signal amplification. But the extended tail sequence at 3′-termins of FS-2 may restrict the target recognition with the TSD probe and the cascade toehold-mediated strand displacement reaction to some extent owing to the steric hindrance, inducing the inferior detection performance toward target DNA compared with that of FS. In the case of FS-3 and FS-4, the detection performance of the biosensor toward target DNA was evidently improved owing to the proximity-based inter-strand displacement effect between the associated fuel strand and the adjacent TSD probe for signal amplification. The dynamic detection range for target DNA by using FS-3 was from 2 fM to 5 pM (Fig. 4C). A linear detection range for target DNA was obtained from 2 to 50 fM with a regression equation of I = −21.79–0.626 C and a regression coefficient of 0.989 (Fig. 5C). Thus,

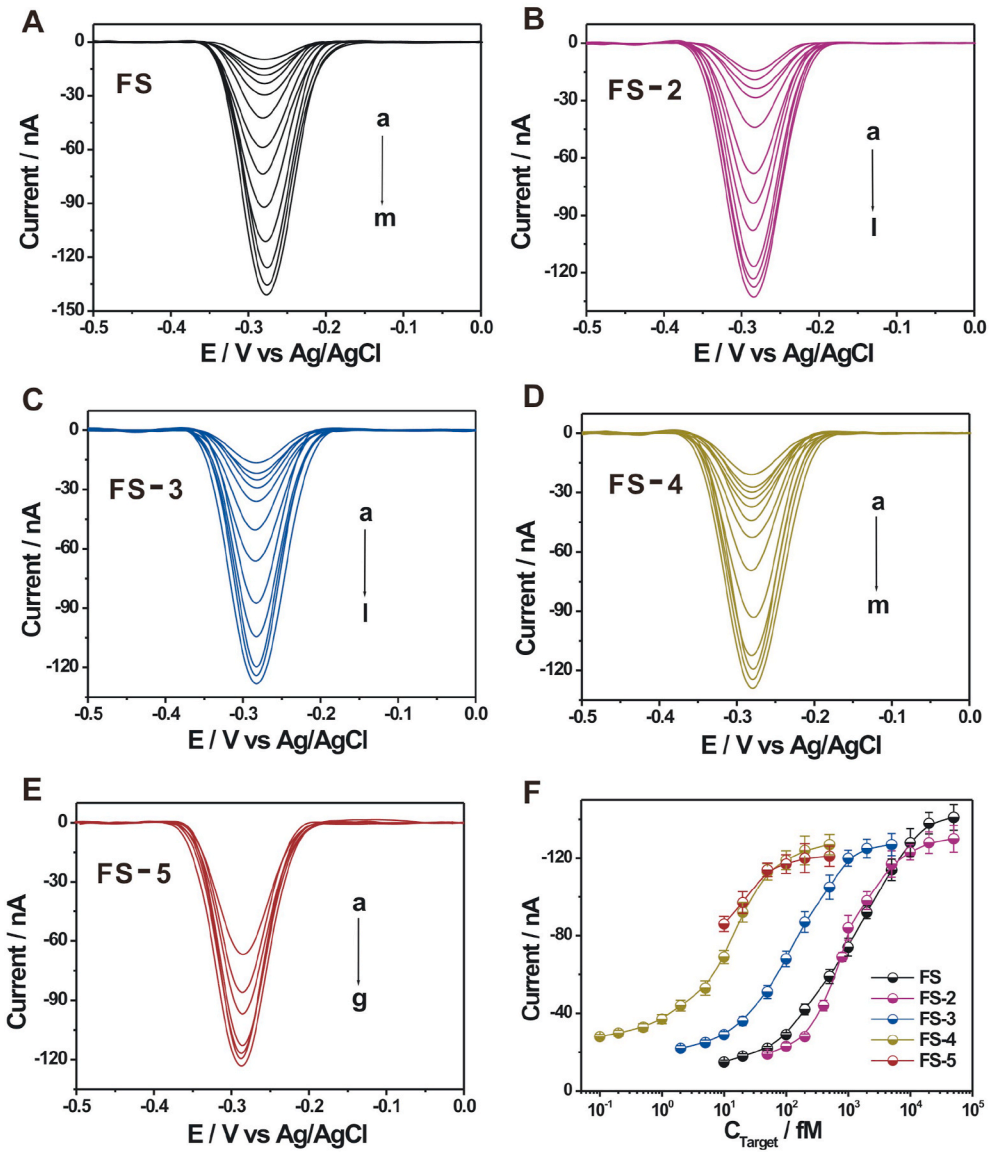


**Fig. 4.** SWV responses toward different concentrations of target DNA by using different fuel strands including FS (A), FS-2 (B), FS-3 (C), FS-4 (D), FS-5 (E). In Fig. 4A, target DNA concentrations (from curves a to m) were 0, 10 fM, 20 fM, 50 fM, 100 fM, 200 fM, 500 fM, 1 pM, 2 pM, 5 pM, 10 pM, 20 pM, 50 pM. In Fig. 4B, target DNA concentrations (from curves a to l) were 0, 50 fM, 100 fM, 200 fM, 400 fM, 800 fM, 1 pM, 2 pM, 5 pM, 10 pM, 20 pM, 50 pM. In Fig. 4C, target DNA concentrations (from curves a to l) were 0, 2 fM, 5 fM, 10 fM, 20 fM, 50 fM, 100 fM, 200 fM, 500 fM, 1 pM, 2 pM, 5 pM. In Fig. 4D, target DNA concentrations (from curves a to m) were 0, 0.1 fM, 0.2 fM, 0.5 fM, 1 fM, 2 fM, 5 fM, 10 fM, 20 fM, 50 fM, 100 fM, 200 fM, 500 fM. In Fig. 4E, target DNA concentrations (from curves a to g) were 0, 10 fM, 20 fM, 50 fM, 100 fM, 200 fM, 500 fM. (F) The calibration plots between SWV current and target DNA concentration by using different fuel strands. The concentrations for all the fuel strands were 0.5 μM.

the target DNA with a low concentration of 2 fM could be detected by using FS-3 as a fuel strand. Furthermore, in the case of FS-4, the best electrochemical detection performance toward target DNA could be achieved. It showed a dynamic response range from 0.1 fM to 500 fM (Fig. 4D). A linear relationship was obtained for the SWV peak current versus target DNA from 0.1 fM to 2 fM with a regression equation of $I = -27.66–8.64\ C$ and a regression coefficient of 0.9904 (Fig. 5D). Thus, a very low target DNA concentration of 0.1 fM could be detected by using FS-4 as the fuel strand. The detection sensitivities of the developed sensing system toward target DNA were obtained as about −4.62, −2.13, −19.94 and −275.16 nA $fM^{-1}$ $cm^{-2}$, respectively, by using the fuel strands of FS, FS-2, FS-3 and FS-4 (Table S2). Thus, the FS-4 could show the best detection sensitivity and a lowest detection limit toward target DNA. In the case of FS-5 as the fuel strand, since the FS-5 could directly trigger the toehold-mediated strand displacement reaction with the TSD probe, the response range toward target DNA was only obtained from 10 fM to 500 fM (Fig. 4E). Also, a very large background response in this case made the FS-5 to be not suitable for target DNA detection. The detection performance of the developed DNA biosensor was compared with those reported methods (Table S3). The low detection limit toward target DNA, especially 0.1 fM by using FS-4, was superior to most of the reported methods. Although the linear range by using FS-4 was relatively narrow, the linear response range of the developed biosensor could be interestingly tuned by using different fuel strands (10–200 fM by FS, 50 fM-1pM by FS-2, 2–50 fM by FS-3 and 0.1–2 fM by FS-4), making the current strategy to be promising for different analysis requirements.

### 3.5. *Selectivity, reproducibility and stability of the fabricated electrochemical DNA biosensor*

The developed fuel strand-powered target recycling and inter-strand displacement strategy was also used to explore its detection selectivity toward different nucleic acids including non-complementary nucleic acid sequence (NC), single-base mismatched sequence (1 MT), three-base mismatched sequence (3 MT). It could be seen from Fig. 5E that the electrochemical responses toward NC and 3 MT were basically similar with the background response. After subtracting the background value, the electrochemical response toward 1 MT was about 19% of that for complementary target DNA. Its good detection selectivity especially for the mismatched bases might be attributed that the mismatched base positioned at the toehold region would evidently inhibit the initial toehold-mediated strand displacement rate and then the fuel strand-powered target recycling and proximity-based inter-strand

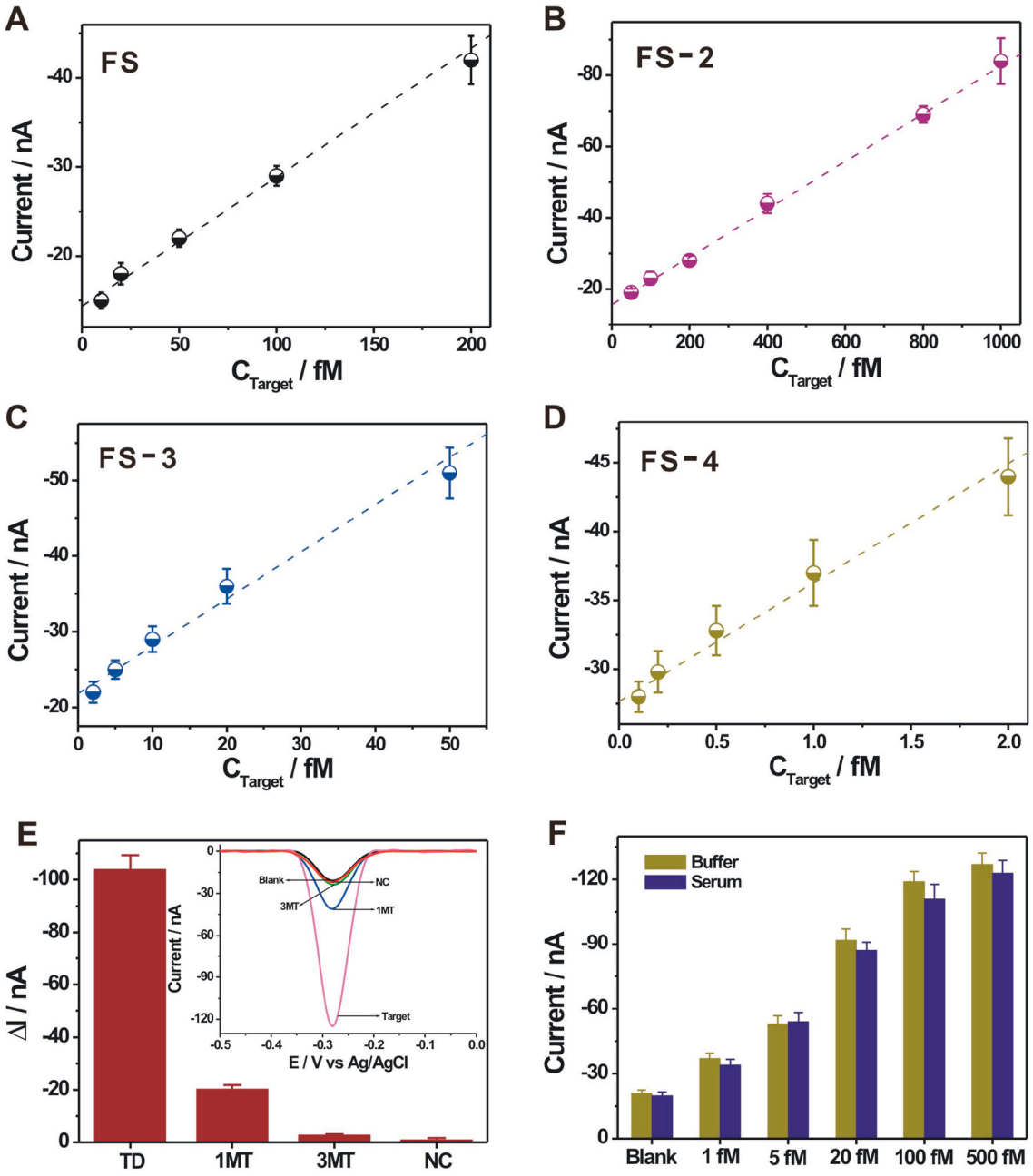


**Fig. 5.** Line relationships between SWV peak current and target DNA concentration by using FS (A), FS-2 (B), FS-3 (C) and FS-4 (D). Target DNA concentrations in Fig. 5A were from 10 to 200 fM. Target DNA concentrations in Fig. 5B were from 50 to 1000 fM. Target DNA concentrations in Fig. 5C were from 2 to 50 fM. Target DNA concentrations in Fig. 5D were from 0.1 to 2 fM. The concentrations for FS, FS-2, FS-3 and FS-4 were 0.5 μM. Error bar for each point was obtained based on at least three repetitive measurements. (E) Electrochemical signal response ($\Delta I = I–I_0$; I and $I_0$ represents the electrochemical signal in the presence and absence of DNA, respectively) toward target DNA against other nucleic acids including 1 MT, 3 MT, NC at 0.2 pM. Inset shows the corresponding SWV responses obtained at different DNAs. (F) The electrochemical responses obtained at different concentrations of target DNA spiked in 10% diluted fetal calf serum and buffer solution. The FS-4 (0.5 μM) was used as the fuel strand in Fig. 5E and F. Error bars represent standard deviations of at least three measurements.

displacement process for the signal decrease.

The applicative potential of the fabricated biosensor for DNA detection in the relatively complex biological matrix was also studied by using the diluted serum as the biological sample. The fetal bovine serum was 10-fold diluted to avoid the possible interference of the biological components toward the biosensor. Then different concentrations of target DNA were spiked into the diluted serum to obtain the model biological sample. The experimental results were shown in Fig. 5F. The electrochemical responses of the fabricated DNA biosensor increased with the increasing concentrations of spiked target DNA in the diluted serum. Generally, the electrochemical responses were only slightly lower than that in the buffer. Thus, the interferences from some possible proteins, ions or other bio-components in the diluted serum for DNA detection were relatively limited, indicating the applicative feasibility of the developed DNA biosensor in the relatively complex biological matrix. Furthermore, the developed sensing strategy may be promising for the nucleic acid detection in various real biological samples for example some disease-related nucleic acid biomarkers in the serum or plasma, various pathogens in biological samples, etc. For it, the TSD probe and fuel strand should be designed toward those specific nucleic acid sequences existed in the biological samples according to the proposed design principle. Before detection, the DNA extraction and heat-

denaturation steps may be combined to obtain the corresponding DNA samples. After the addition of fuel strand into the DNA samples and incubation with the TSD probe modified electrode, the electrochemical interrogation was conducted for signal reading related with target information. It may be also directly employed for the detection of cell-free DNA or microRNA in the serum or plasma.

The detection reproducibility of the fabricated DNA biosensor toward target DNA by using FS-4 as the fuel strand was checked. The relative standard deviations for the detection of 0.5 fM, 5 fM and 0.1 pM target DNA were obtained as about 5.48%, 6.82% and 4.1%, respectively, by using four different electrodes prepared under the same experimental conditions for each sample (Fig. S4A). Furthermore, the storage stability of the constructed DNA biosensor was examined. When, the TSD probe modified electrode was kept at 4 °C for two weeks, the electrochemical intensity toward 0.2 pM target DNA by using FS-4 as the fuel strand decreased less than 10%. These results demonstrated the satisfactory reproducibility and stability of the developed DNA biosensor.

## 4. Conclusions

A fuel strand-powered self-propelled electrochemical DNA machine was well constructed for enzyme-free and autocatalytic detection of nucleic acid. In current strategy, the fuel strand was simply configured with a tail sequence that could act as a target analogy. It thus could execute for target DNA detection besides the typical fuel strand-powered target recycling for signal amplification, the tail sequence of the associated fuel strand could be used as a DNA walker to trigger the proximity-based inter-strand displacement for the self-propelled signal amplification. The detection performance (dynamic response range, linear interval and detection limit) could be interestingly tuned by changing the tail sequence length of fuel strands added in the sample based on the same biosensing interface, showing the potential to satisfy different analysis requirements. It showed the low detection limit toward the same target DNA sequence of about 10 fM, 50 fM, 2 fM and 0.1 fM, respectively, by using fuel strands of FS, FS-2, FS-3 and FS-4. The current self-propelled DNA machine also demonstrated the advantages of enzyme-free, facile sequence design, and one-step assay process. Thus, it might hold a great potential as a competitive signal amplification means to construct various biosensing system for a broad of applications in disease diagnosis and clinical biomedicine.

## CRediT authorship contribution statement

**Zhen Zhao:** Methodology, Investigation, Writing - original draft. **Zhiqiang Chen:** Investigation, Visualization, Data curation. **Dengren Liu:** Software, Formal analysis. **Li Wang:** Validation, Data curation. **Shufeng Liu:** Conceptualization, Writing - review & editing, Supervision.

## Declaration of competing interest

The authors declare that they have no known competing financial interests or personal relationships that could have appeared to influence the work reported in this paper.

## Acknowledgements

We acknowledged the finance supports from the Natural Science Foundation of Shandong Province (No. JQ201704) and National Natural Science Foundation of China (No. 21475072).

## Appendix A. Supplementary data

Supplementary data to this article can be found online at https://doi.org/10.1016/j.bios.2020.112706.

## References

Bachman, J., 2013. Methods Enzymol. 530, 67–74.
Bath, J., Turberfield, A.J., 2007. Nat. Nanotechnol. 2, 275–284.
Chen, J., Qiu, H., Zhang, M., Gu, T., Shao, S., Huang, Y., Zhao, S., 2015. Biosens. Bioelectron. 68, 550–555.
Chu, Y., Deng, A.P., Wang, W., Zhu, J.J., 2019. Anal. Chem. 91, 3619–3627.
Craw, P., Balachandran, W., 2012. Lab Chip 12, 2469–2486.
Dai, J., He, H., Duan, Z., Guo, Y., Xiao, D., 2017. Anal. Chem. 89, 11971–11975.
Das, J., Ivanov, I., Montermini, L., Rak, J., Sargent, E.H., Kelley, S.O., 2015. Nat. Chem. 7, 569–575.
Dirks, R.M., Pierce, N.A., 2004. Proc. Natl. Acad. Sci. U.S.A. 101, 15275–15278.
Gerasimova, Y.V., Kolpashchikov, D.M., 2014. Chem. Soc. Rev. 43, 6405–6438.
Hindson, C.M., Chevillet, J.R., Briggs, H.A., Gallichotte, E.N., Ruf, I.K., Hindson, B.J., Vessella, R.L., Tewari, M., 2013. Nat. Methods 10, 1003–1005.
Jung, C., Ellington, A.D., 2014. Acc. Chem. Res. 47, 1825–1835.
Khodakov, D.A., Khodakova, A.S., Linacre, A., Ellis, A.V., 2013. J. Am. Chem. Soc. 135, 5612–5619.
Kim, D., Garner, O.B., Ozcan, A., Carlo, D.D., 2016. ACS Nano 10, 7467–7475.
Li, F., Tang, Y., Traynor, S.M., Li, X.F., Le, X.C., 2016. Anal. Chem. 88, 8152–8157.
Lin, M., Song, P., Zhou, G., Zuo, X., Aldalbahi, A., Lou, X., Shi, J., Fan, C., 2016. Nat. Protoc. 11, 1244–1263.
Liu, S., Fang, L., Wang, Y., Wang, L., 2017. Anal. Chem. 89, 3108–3115.
Liu, S., Xin, C., Yu, X., Ding, Z., Liu, S., 2019. Analyst 144, 5923–5927.
Liu, S., Yu, X., Wang, J., Liu, D., Wang, L., Liu, S., 2020. Anal. Chem. 92, 9764–9771.
Mahshid, S.S., Camiré, S., Ricci, F., Vallée-Bélisle, A., 2015. J. Am. Chem. Soc. 137, 15596–15599.
Navarro, E., Serrano-Heras, G., Castaño, M.J., Solera, J., 2015. Clin. Chim. Acta 439, 231–250.
Qian, L., Winfree, E., 2011. Science 332, 1196–1201.
Qu, X., Zhu, D., Yao, G., Su, S., Chao, J., Liu, H., Zuo, X., Wang, L., Shi, J., Wang, L., Huang, W., Pei, H., Fan, C., 2017. Angew. Chem. Int. Ed. 56, 1855–1858.
Shang, J., Wei, J., Wang, Q., Wang, J., Zhou, Y., Yu, S., Liu, X., Wang, F., 2020. Biosens. Bioelectron. 152, 111994.
Shen, Z.F., Li, F., Jiang, Y.F., Chen, C., Xu, H., Li, C.C., Yang, Z., Wu, Z.S., 2018. Anal. Chem. 90, 3335–3340.
Simmel, F.C., Yurke, B., Singh, H.R., 2019. Chem. Rev. 119, 6326–6369.
Srinivas, N., Ouldridge, T.E., Sulc, P., Schaeffer, J.M., Yurke, B., Louis, A.A., Doye, J.P.K., Winfree, E., 2013. Nucleic Acids Res. 41, 10641–10658.
Steel, A.B., Herne, T.M., Tarlov, M.J., 1998. Anal. Chem. 70, 4670–4677.
Sun, X., Wei, B., Guo, Y., Xiao, S., Li, X., Yao, D., Yin, X., Liu, S., Liang, H., 2018. J. Am. Chem. Soc. 140, 9979–9985.
von Delius, M., Leigh, D.A., 2011. Chem. Soc. Rev. 40, 3656–3676.
Wang, H., Li, C., Liu, X., Zhou, X., Wang, F., 2018a. Chem. Sci. 9, 5842–5849.
Wang, K., Feng, M., He, M.Q., Zhai, F.H., Dai, Y., He, R.H., Yu, Y.L., 2018b. Talanta 188, 685–690.
Xiong, E., Zhen, D., Jiang, L., Zhou, X., 2019. Anal. Chem. 91, 15317–15324.
Yang, J., Wu, R., Li, Y., Wang, Z., Pan, L., Zhang, Q., Lu, Z., Zhang, C., 2018. Nucleic Acids Res. 46, 8532–8541.
Yang, X., Tang, Y., Mason, S.D., Chen, J., Li, F., 2016. ACS Nano 10, 2324–2330.
Yao, D., Bhadra, S., Xiong, E., Liang, H., Ellington, A.D., Jung, C., 2020. ACS Nano 14, 4007–4013.
Yin, P., Choi, H.M.T., Calvert, C.R., Pierce, N.A., 2008. Nature 451, 318–322.
Yun, W., Jiang, J., Cai, D., Zhao, P., Liao, J., Sang, G., 2016. Biosens. Bioelectron. 77, 421–427.
Yurke, B., Turberfield, A.J., Mills, A.P., Simmel, F.C., Neumann, J.L., 2000. Nature 406, 605–608.
Zhang, D.Y., Turberfield, A.J., Yurke, B., Winfree, E., 2007. Science 318, 1121–1125.
Zhou, R., Hu, C., Jin, Y., Zhang, J., Du, H., Yang, P., Chen, J., Hou, X., Cheng, N., 2020. Anal. Chem. 92, 8909–8916.
Zhu, J., Zhang, L., Li, T., Dong, S., Wang, E., 2013. Adv. Mater. 25, 2440–2444.